Three modes of electrochemical impedance spectroscopy measurements performed on vanadium redox flow battery

Joanna Krakowiak[1,*], Wojciech Bącalski[1], Grzegorz Lentka[2], Pekka Peljo[3], Paweł Ślepski[1]

[1] Chemical Faculty, Gdańsk University of Technology, ul. Narutowicza 11/12, 80-233 Gdańsk, POLAND;
[2] Faculty of Electronics, Telecommunications and Informatics, Gdańsk University of Technology, ul. Narutowicza 11/12, 80-233 Gdańsk, POLAND;
[3] Research Group of Battery Materials and Technologies, Department of Mechanical and Materials Engineering, Faculty of Technology, University of Turku, 20014 Turun Yliopisto, Finland
* corresponding author: joakrako@pg.edu.pl

Abstract

This article presents an innovative approach to monitor working redox flow batteries using dynamic electrochemical impedance spectroscopy, diverging from the commonly sequential impedance methods carried out under potentiostatic or galvanostatic conditions close to the open circle voltage. The authors introduce a fresh variation of dynamic impedance measurement that leverages an amplitude-modulated multi-frequency alternating current perturbation signal. This technique leads to a reduction in measurement time, making it possible to monitor impedance in real-time under typical operational conditions. Consequently, it effectively addresses the limitations stemming from the absence of stationary conditions during impedance measurements. There is no doubt that measurement techniques enabling the study of processes during the operational life of a battery provide the most valuable insights into the properties of these systems. The potential of this proposed approach is exemplified through the examination of a full vanadium redox flow battery as a case study. Classical impedance measurements were also conducted under potentiostatic and galvanostatic conditions with sequential frequency signal change, which requires stopping the battery operation, resulting in electrode potential changes of over 200 mV compared to the working system. Spectra for all modes of measurements were compared. In the case of dynamic measurements, such significant differences in spectra during charging and discharging are not observed, which is characteristic of classical measurements. The authors deliberately and consciously refrain from analyzing the results by fitting equivalent circuits.

KEYWORDS: energy storage; redox flow battery; dynamic impedance; nonstationary conditions, real time monitoring

1. Introduction

Stationary electrochemical energy storage systems are important today and will become increasingly important and necessary in the future for several reasons. Firstly, the growing demand for renewable energy, such as solar and wind power, requires increased ability to store electrical energy for use when sources

are not available or generating low power. Stationary electrochemical energy storage systems are capable of storing electrical energy in a way that allows for use when needed. Secondly, energy grid stability can be improved with energy storage systems, especially in cases of increased use of renewable energy. Electrochemical energy storage systems can help to provide energy when the grid is under load or when irregularities in energy supply occur. Thirdly, energy efficiency can be increased with stationary electrochemical energy storage systems, which can lead to reduced greenhouse gas emissions. They allow for energy to be stored when it is available in excess and then used during peak times or when energy is not available. All these factors make stationary electrochemical energy storage systems important and increasingly necessary in the future. The redox flow battery (RFB) is an energy storage technology that holds potential for large-scale applications due to its unique benefits, such as extended lifespan, straightforward design, separated power and energy, among others. Some RFB systems, such as all-vanadium RFBs (VRFB), have been successfully commercialized. Nevertheless, the relatively low energy density remains a disadvantage of these systems. As a result, numerous innovative RFB systems have been developed to address this issue and improve overall performance and efficiency.

Elucidating the structure and composition of energy materials and their reaction mechanisms is crucial to the design of advancing energy storage technologies. The application of modern *in situ/operando* techniques has been a source of valuable insights for establishing composition-reactivity correlations under real-time reaction conditions. This provides significantly more insight into function compared to isolated and simplified laboratory conditions.

Electrochemical impedance spectroscopy (EIS) has the advantage of being no-destructive, fast and even standardly used to analyze electrochemical processes. This technique has witnessed a significant surge in popularity in recent years. Initially utilized for determining double-layer capacitance and in AC polarography, it is now extensively employed in the characterization of electrode processes and complex interfaces. To make an EIS measurement, the alternating current (AC) signal (voltage or current) is applied at a constant voltage (potentiostatic) or constant current (galvanostatic) and the response is measured[1]. The impedance Z is determined by the frequency-dependent voltage/potential $V(\omega)/E(\omega)$ and frequency-dependent current $I(\omega)$. The validity of EIS is assessed by considering three primary factors: linearity, stationarity, and causality. The authors do not intend to present in detail this measurement technique, as such information is available in numerous books and scientific articles[2–5]. We focus only on selected aspects to provide an introduction to the applied measurement technique.

EIS contains analyzable information at each frequency because different overvoltage contributions evolve on different time scales and it can directly measure physical or chemical processes like electrochemical activity, kinetics, adsorption or diffusion. For example, the charging of the electrochemical double-layer usually occurs on the microseconds time scale, but diffusion can be observed on the hundreds of milliseconds

time scale (Figure 1). Valid Nyquist plots should be repeatable, show characteristic processes taking place in the battery and do not have noise.

The electrochemical process is usually approximated by an equivalent circuit model composed of resistors, capacitors, inductors, and specific parts like these considering diffusion. These elements can represent the physicochemical processes in the system and their values are acquired by matching the mathematical equation underlying the circuit model to the impedance spectra obtained through experimentation. Both modes (potentiostatic and galvanostatic) usually generate equal results if the electrochemical properties of the system do not change over the measurement time. The use of galvanostatic mode further complicates the measurement due to often unsatisfactory accuracy of the obtained results and lack of control over the potential, which frequently leads to uncontrolled polarization of the studied system. Measurements in galvanostatic mode are much less frequently conducted because obtaining accurate results requires the application of a complex and diverse amplitude-controlled sequential excitation[6].

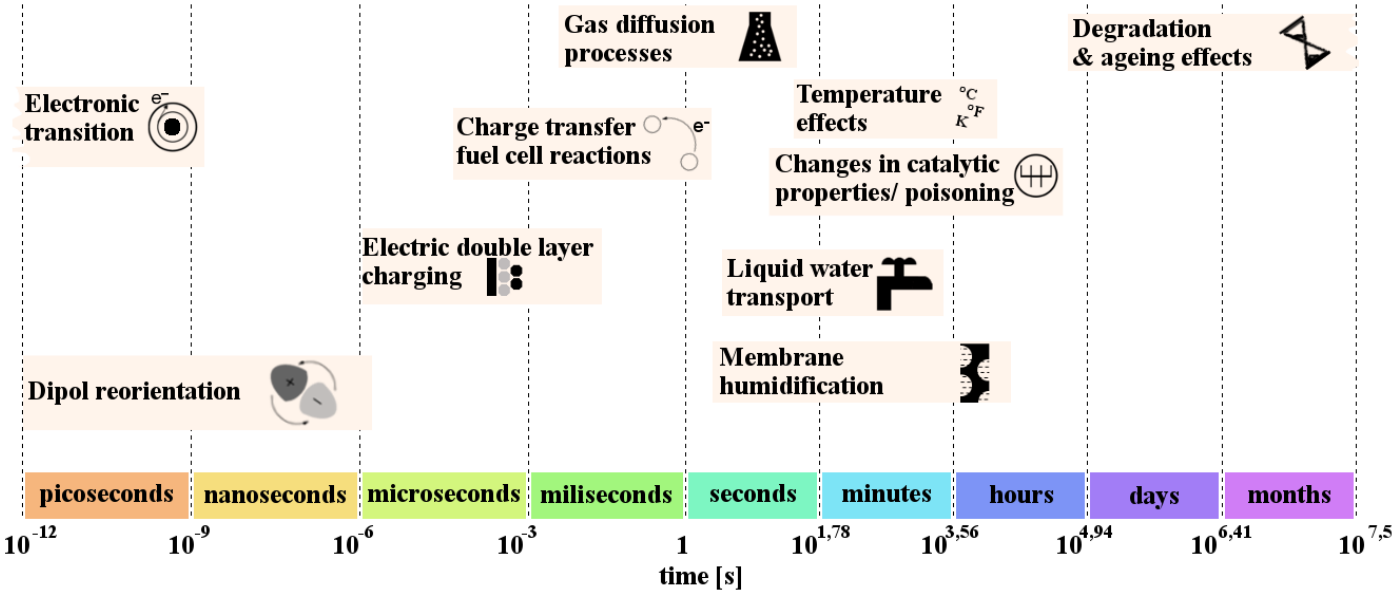

Figure 1. The illustrative range of time scales for chemical and physical process which can occur in electrochemical systems.

Numerous equivalent circuits for studied systems have been proposed[7]. However, equivalent circuits drawn for electrochemical cells are not unique and given experimental data can be covered by different electrochemical models. It's important to note that in most cases, it is not possible to directly associate specific circuit components with the processes taking place within the cell.

Electrochemical Impedance Spectroscopy is one of the most useful techniques for characterizing and modeling batteries as it can provide detailed information on physico-chemical processes that arise inside the battery: electrochemical mechanisms, reaction kinetics, battery life performance, state of charge, features of electrode materials, state of health (SOH) or the factors responsible for the loss of capacity[8]. In the case of the most widespread lithium-ion batteries galvanostatic mode is recommended[9]. Additionally

the literature review indicates that the application of various impedance measurement modes has been extensively analyzed and examined for lithium-ion batteries[9–11]. Hence, it seems justified to draw inspiration from these studies, as well as those dedicated to fuel cells, due to the significant analogy in their construction and operation.

To date, almost all existing scientific literature discusses impedance measurements for RFB with single cells. Such impedance measurements were mostly obtained during the potentiostatic control mode at an equilibrium state after the cell has reached a given state of charge (SoC) both for aqueous[12–14] and nonaqueous[15–17] systems. Many studies deal with a modification of the electrodes through chemical or physical processes and the EIS test is often the main method verifying the change of the battery parameters performance[18–22]. The effects of membrane[23], current density, electrolyte solution flow rate, and ion type or concentration on a impedance of the battery were also analyzed, as well as the influence of over-charge on ohmic impedance[24–26].

Table 1. The components of different modes for electrochemical impedance spectroscopy investigations. The measurement modes employed in the experimental section are underlined for clarity.

Electrochemical Impedance Spectroscopy	**Input-output signals**	Potentiostatic	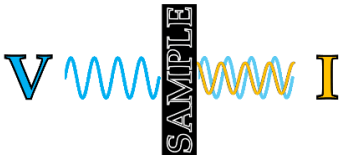
		<u>Galvanostatic</u>	
	Current-voltage relation	<u>Linear</u>	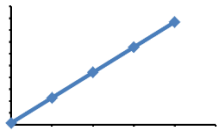
		Non-linear	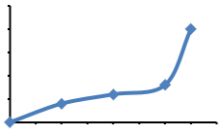
	Used frequencies of excitation signal	Sequential	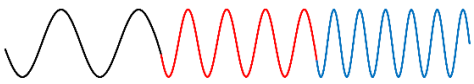
		<u>Multi-sinusoidal</u>	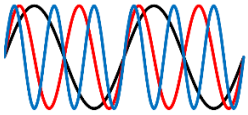

EIS measurements were also conducted and were observed to be repeatable for flow battery with large sized electrodes and multiple cells[27]. The response time was investigated in two kilowatts-class (kW-class) batteries[28] by this technique. Such analysis is essential for design of the grid services. Trovò[29] introduces a multichannel Electrochemical Impedance Spectroscopy system designed for high bias current operation, specifically tailored for kW-class Vanadium Redox Flow Batteries.

The measurement time for typical EIS investigations is particularly lengthy, especially at low frequencies, when utilizing a series of single-frequency excitation signals, which can compromise the stationarity of the battery system. To expedite the EIS measurement process, multisine signals encompassing a broad range of frequencies can be employed. These signals are composed by a summation of sine (or cosine) waves[10].

Recent advances in electrochemical impedance spectroscopy shows the capability of acquiring impedance spectra of non-stationary systems in a broad range of frequencies by applying a perturbation with a package of sinusoids and joint time–frequency analysis of the response signal. Table 1 presents the components of the mode applicable to various variants of impedance measurements. Currently, measurements can be performed in any combination of the presented measurement modes. For convenience, the measurement modes used in the experimental part have been highlighted in the table.

The implementation of a multi-sinusoidal excitation signal for the first time was applied by Smith and Creason [30] in the 1970s. Next, Short-Time Fourier Transform (STFT) was utilized for obtaining impedance changes in the time domain from given local parts of the spectrum[31,32]. Over this period, it has found incredibly broad applications, as evidenced by the number of published reports[33,34,43,44,35–42], but it has not been commercialized. Some papers have proven that this method is an excellent tool for monitoring of the working electrochemical batteries[45,46]. Continuous impedance measurements can be performed simultaneously using the range of pseudo-white noise method, what allows to determine the cell parameters under any charge and discharge modes, even during its exploitation condition for chosen frequencies. Slepski presents the principles of the measurement, which allows to obtain a full impedance characteristic of cells and single electrodes[47]. However, it's worth introducing some information. The main disadvantage of sequential stimulation is the long duration (t) required to obtain the impedance spectrum, which depends on both the number of analyzed frequencies (f_i) and the number of periods generated for each sinusoid (n):

$$t = \sum_{i=0}^{k} (n/f_i) \tag{2}$$

A spectacular reduction in measurement time is achieved by using multi-sinusoidal excitation, where all sinusoidal signals are generated simultaneously. In current-controlled conditions, this signal can be represented as follows:

$$I_{ac} = \begin{bmatrix} i_1 sin(2\pi f_1 \tau + \varphi_1) \\ i_2 sin(2\pi f_2 \tau + \varphi_2) \\ \dots \\ i_{k-1} sin(2\pi f_{k-1} \tau + \varphi_{k-1}) \\ i_k sin(2\pi f_k \tau + \varphi_k) \end{bmatrix} \quad (3)$$

In this case, the duration of the excitation (t) required to determine a single spectrum is given by the following relationship:

$$t = n/f_k \quad (4)$$

As can be seen, the measurement time is reduced to the period in which the component with the lowest frequency (f_k) is generated. This significantly increases the possibility of maintaining steady-state conditions during the period from which the impedance spectrum is obtained.

In cases where the studied system exhibits non-stationarity during the measurement, using multi-sinusoidal excitation, as opposed to sequential excitation, often allows obtaining an interpretable characteristic of the object. This feature can be explained by considering a simple system represented by two elements (capacitor and resistor connected in parallel - C_1R_2), where the value of C_1 is constant, while the value of R_2 decreases over time. The impedance spectrum of such a system in the form of Nyquist plot is shown in Figure 2a. In the case of using classical sequential excitation, where the successive analyzed frequencies are progressively lower, the impedance spectrum of the considered system will approximately have a shape reflected in the Figure 2a. Analyzing such obtained impedance spectrum is impossible using a real equivalent circuit (C_1R_2). Using any other circuit model will result in an incorrect interpretation of the analyzed phenomenon (Figure 2b). A different situation arises when using a multi-sinusoidal signal. The analysis of the excitation signal and response is carried out in this case using Fourier transformation. The averaging nature of the transformation, from the time domain to the frequency domain, results in the obtained impedance spectrum representing an average over the measurement period (Figure 2c). The spectrum obtained in this way accurately represents the studied system during the measurement and, when using the correct equivalent circuit, allows obtaining the real/average parameters of the system.

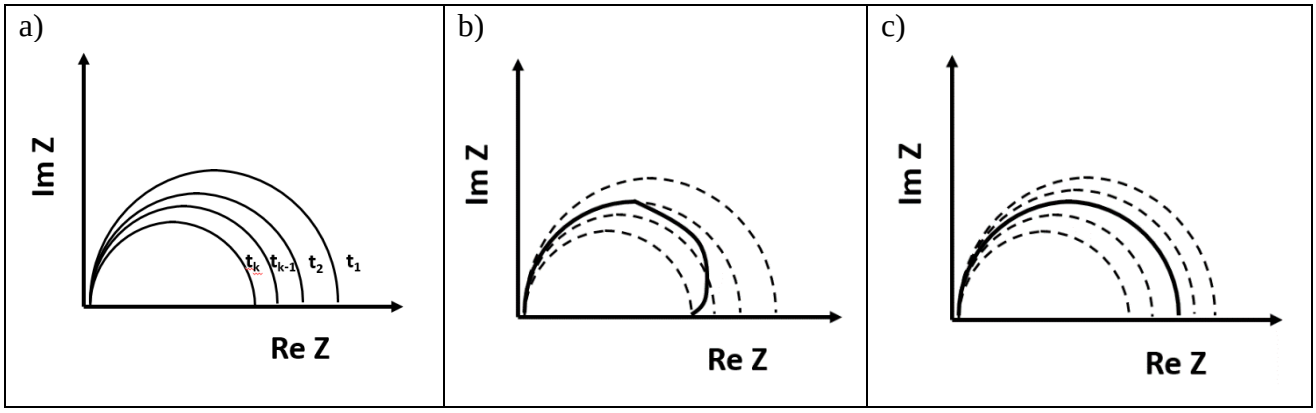

Figure 2. Exemplary impedance spectra of the (C_1R_2) system with R_2 value decreasing with time; a) real spectra; b) spectra obtained for sequences change of frequency – the solid line; c) spectra recorded for multi-sinusoidal excitation – the solid line.

For excitation signal, the magnitude of the resultant amplitude depends on both the amplitudes of the components of the multi-sinusoidal signal and the phase shifts between successive components. The multi-sinusoidal signal should have the lowest possible amplitude to avoid undesired changes in the analyzed system.

In the case of multi-sinusoidal excitation, the full frequency range (from megahertz to millihertz) is currently not utilized due to technical reasons. When using the sum of elementary sinusoidal signals as the excitation signal, the following aspects determining the frequency range should be taken into account: (i) the frequency range in which electrode processes occurring in the studied system are detected, (ii) the dynamics and duration of the analyzed electrode process, and (iii) the measurement capabilities of the measurement system used. When selecting individual frequency components, it is also important to consider that electrochemical systems have a non-linear nature. Each frequency component of the multi-sinusoidal excitation signal can generate additional harmonic components in the response signal. To avoid superposition of harmonic signals with fundamental frequencies, a frequency selection based on prime numbers or their multiples could be applied. When selecting individual frequencies, it is also important to remember that the properties of most electrochemical systems make it advantageous to have a logarithmic distribution of excitation frequency components to obtain the best impedance characterization of the object.

Obtaining the impedance of the studied object requires decomposing the multi-sinusoidal excitation signal and response signal, which provides information about the phases and amplitudes of all sinusoidal components (the idea of this procedure is shown on Figure 3). To achieve this, the recorded voltage and current signals are subjected to Fourier or Laplace transformations. Applying these transformations enables obtaining an averaged impedance characteristic of the system, but temporal localization information is lost in the process. Temporal changes in the system's impedance can be obtained by performing the above operation sequentially on signal segments of a specific length L.

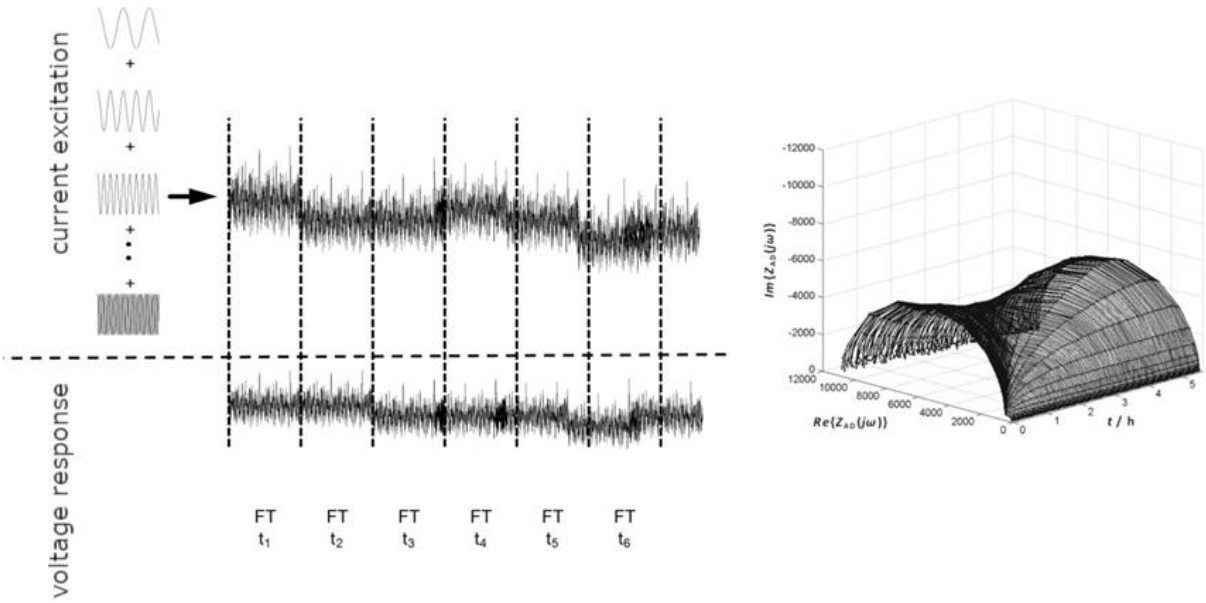

Figure 3. Scheme presenting determination of the impedance in function of time

Such an operation is known as Short-Time Fourier Transform (STFT), which in its discrete form presents as follows:

$$\mathrm{DSTFT}[\mathrm{m},\mathrm{n}] = \sum_{k=0}^{L-1} \mathrm{s}[\mathrm{k}]\gamma^{*}[k-m]exp(-j2\pi kn/L) \tag{5}$$

The above relation assumes that unitary Fourier transformations are performed on segments of length L extracted from the analyzed signal s[k] using windowing functions γ*. This action aims at reducing the phenomenon called spectral leakage, that may lead to partial distortion of the results. Complete elimination of leakage of the spectrum and simplification of the calculation were obtained when using a rectangular window function and proposing to keep the specific relationship between the length of the analysis window L, and the individual frequencies of the analysed multisinusoid signal f_i:

$$f_i = \mathrm{n}\,\mathrm{f_s}/L \quad ,\mathrm{n} = 1,2,\ldots \tag{6}$$

The application of the above condition boils down to preserving the total number of periods of all the multicomponent frequency signal within the analyzed segment of length L.

Even this fairly short presentation of dynamic electrochemical impedance spectroscopy (DEIS) measurements clearly indicates the advantages of this method, which include: (i) a very short measurements time; (ii) the ability to identify and describe physical and chemical processes during cell charging/discharging under any current conditions without the need for stationary current-potential relationships, unlike the highly divergent conditions encountered in classical EIS measurements; (iii) the possibility of observing results in real-time mode, which can serve as a monitoring tool for process correctness in both laboratory and commercial setups. There are surely many other potential applications of this method, which are difficult to

enumerate unambiguously due to the lack of experimental data, on which we are constantly working, and we will promptly inform about new possibilities in subsequent scientific papers.

Continuous simplified DEIS measurements for single frequency during charging/discharging operation has been also used for battery investigation[48].

In this paper, an alternative continuous impedance measurement method is introduced in contrast to the well-established sequential potentiostatic and galvanostatic measurements. The objectives of this study are as follows: (i) to present the first instance of such measurements conducted on a nonstationary redox flow battery system operating in galvanostatic mode; (ii) to highlight the advantages of continuous impedance measurements in cell investigations. All measurements were carried out on a two-electrode system (i.e., the entire cell). The authors have chosen not to analyze the spectra using an equivalent circuit due to the complexity of the entire cell system. Such investigations become particularly valuable when a three-electrode system is employed, allowing for the monitoring of processes occurring at individual electrodes. It is also noted that fitting an equivalent circuit to the entire cell's operation is an inefficient use of effort, especially since it is difficult to attribute physical meaning to individual elements of the system when considering both the complex cathodic and anodic processes. The authors are currently dedicated to modifying the redox flow system to obtain impedance spectra for a single electrode. This aspect will be the focus of a future publication

2. Experimental

2. 1. Redox flow battery

The experiment was performed using a full-vanadium redox flow battery lab-cell . A commercial vanadium electrolyte from GfE, Nürnberg, Germany, was employed, which consisted of a sulfuric acid aqueous solution containing 1.6 M vanadium ions at oxidation state +4 (as VO^{2+} ion) and at oxidation state +3 (as V^{3+}) in equimolar concentration. For the laboratory-scale single-cell VRB system, Rayon-based graphite felt was used for both the negative and positive electrodes. The electrodes were thermally activated in an air atmosphere at 500°C for 9 hours. The electrode area was 500 mm^2 (20x25 mm), and the thickness was 5 mm. Nafion 117 membrane was used to separate the two half-cells, and a peristaltic pump (Watson Marlow 323) was employed to maintain a constant electrolyte flow rate of 40 ml/min. The oxygen was removed from the negative electrolyte by flushing the solution with nitrogen.

2.2. Electrochemical study

The EIS measurements were performed following three charging tests. The charge-discharge measurements were conducted within the voltage range of 1.8 to 0.5 V under direct constant-current conditions. A current of 0.25 A was applied and controlled by a potentiostat-galvanostat (Autolab 302N). The battery state of charge was determined based on the charge that flowed through the battery during its operation.

A typical Electrochemical Impedance Spectroscopy measurement was conducted using a series of single-frequency excitation signals for the frequency range between 10 kHz and 100 mHz. The measurements were performed in both potentiostatic and galvanostatic modes at different states of charge levels: 0%, 25%, 50%, 75%, and 100%.

Impedance spectra were obtained at a specific SoC twice: once during the battery charging process and again during the battery discharging process, using a constant direct current of 0.25 A, which corresponds to a current density of 50 mA/cm^2.

For potentiostatic measurements, the cell was charged or discharged to a specified level of SoC. After stopping the charging or discharging procedure, the open cell voltage was recorded, and the impedance measurement was performed. The sinusoidal excitation signal had an amplitude of 10 mV,

For galvanostatic measurements, the cell was charged or discharged to a specified level of SoC, and the impedance measurement was performed without any interruption in the charging or discharging process. The sinusoidal excitation signal had an amplitude of 25 mA.

A continuous impedance measurement, during the charging and discharging process, was carried out using a National Instruments PXI-4461 card generating a multisinusoidal perturbation signal and recording current and voltage response. This AC signal was added to the DC (direct current) component of the charge/discharge current generated by the Autolab 302N. The analysed frequency range was 4.5 kHz to 0.3 Hz. The amplitudes and phase shifts of the individual excitation components were selected so that the resulting response signal did not exceed ±25mV. Control and analysis of the recorded signals was carried out using appropriate programs prepared in LabView.

3. Results and discussion

The experiment started with charge-discharge performances of the VRFB system. The last four cycles are presented in the Figure 4. The columbic and voltage efficiencies of the presented cycles are practically identical and amount to 89.6% and 67.9%, respectively.

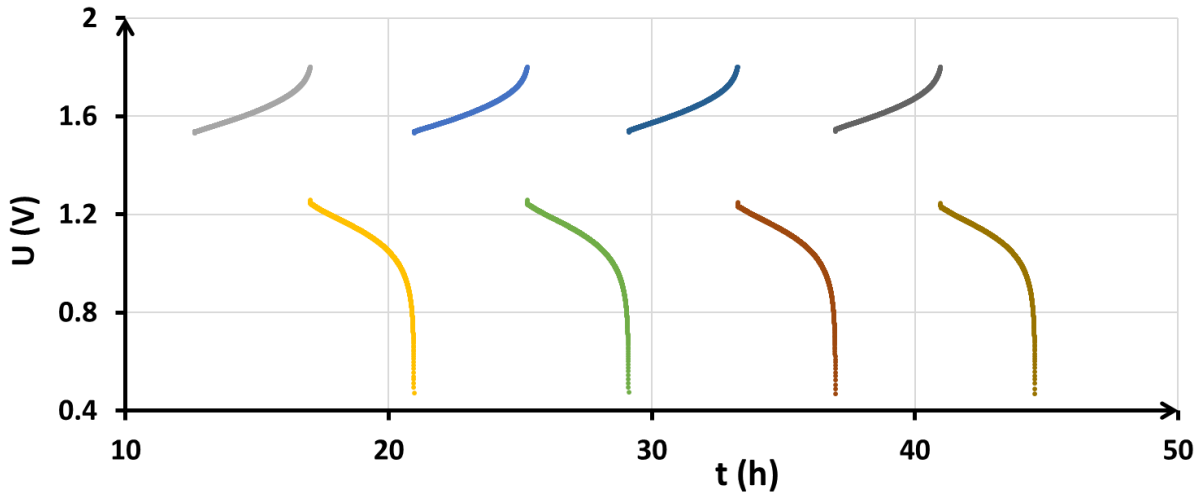

Figure 4. The charge-discharge performance for VRFB system at constant density current of 50mA/cm^2. The columbic and voltage efficiencies are 89.6% and 67.9%, respectively and differ slightly, within the measurement error.

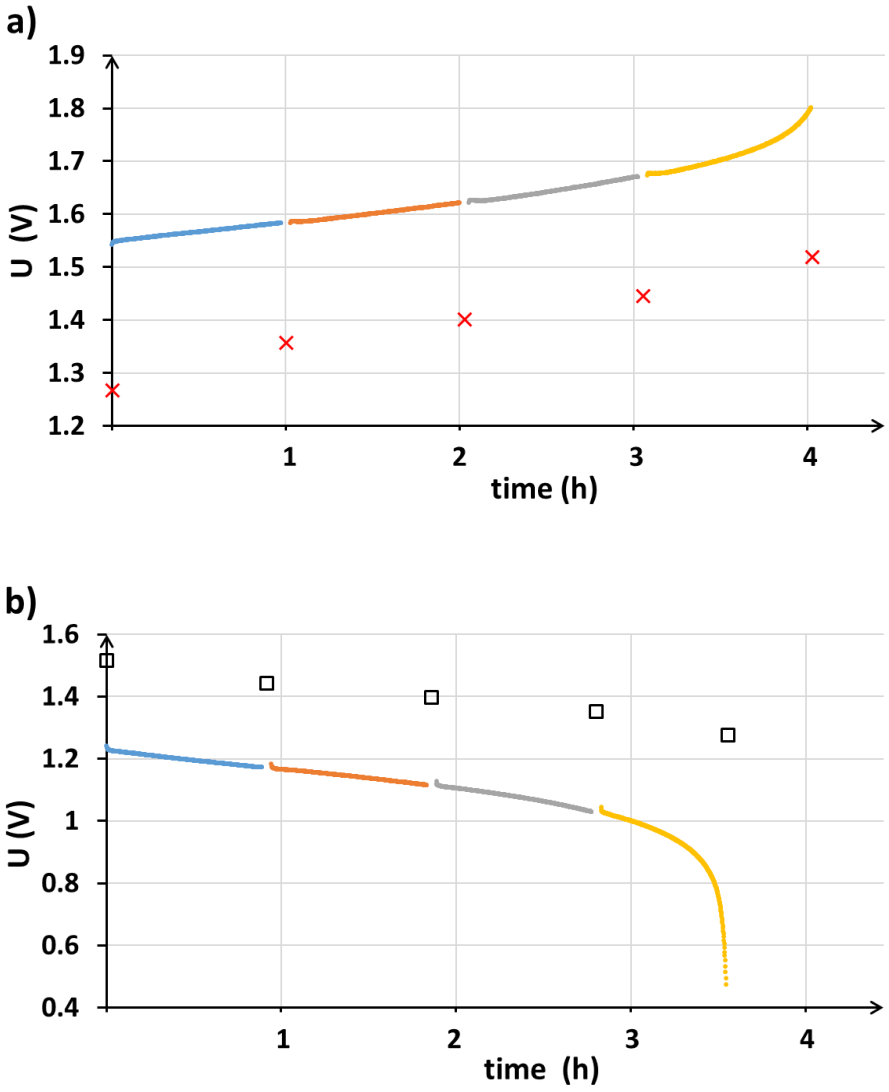

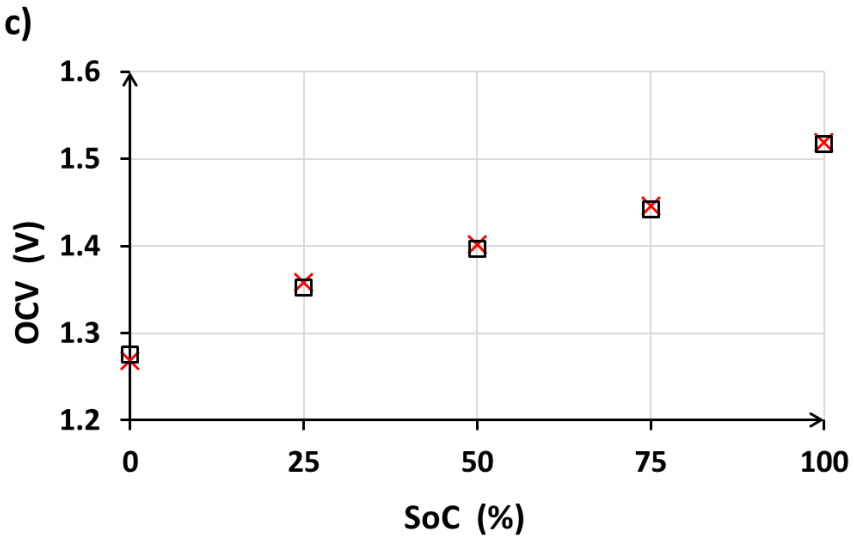

Figure 5. The charge (a) and discharge (b) curves for the VRFB, as well as the OCV values determined prior to potentiostatic EIS measurements during charging (x) or discharging (□) interruptions; the OCV values (c) during charging (x) or discharging (□) interruptions against the SoC values.

As mentioned earlier, potentiostatic impedance measurements were conducted between the charging or discharging processes to a predetermined state of charge of the battery. This implies that the electrode condition during the electrochemical impedance spectroscopy measurement differs from that obtained during charging or discharging at the same SoC level. Figures 5a and 5b depict the charge-discharge curves and the voltage of the cell (open circuit voltage, OCV) during the EIS measurement.

It is evident that significant differences exist between the cell voltage during charging or discharging and the OCV value at a given SoC. This difference amounts to at least 220mV, which is substantial in terms of electrochemical reaction behavior. This discrepancy represents a significant disadvantage of the potentiostatic mode of impedance spectroscopy because the measurement is conducted at a voltage far from the actual voltage within the working cell. The Figure 5c shows the OCV values during charging or discharging interruptions against the state of charge. As it can be seen, a very good repeatability is observed between presented data and like for most electrochemical systems the equilibrium potential is unambiguously defined by the state of charge.

During the operation of a VRFB, various electrochemical phenomena take place. Ohmic polarization arises due to the resistance encountered by the membrane, liquid electrolyte, and the electrode material between the bipolar plates. Mass transfer polarization occurs as the electrolyte flows through the porous felt electrodes. Charge transfer polarization can be observed at the anode and cathode electrodes, arising from electrode activity, electrolyte-coupled reactions (reactions dependent on the wetting of the electrode surface by the electrolyte), and charge transfer within the liquid electrolyte. These phenomena influence the impedance value within a specific frequency range. Figure 6 displays Nyquist plots obtained

in the potentiostatic mode at various levels of state of charge: 0%, 25%, 50%, 75%, and 100% attained during charging or discharging interruptions. It is evident and well known that the spectra change with SoC level. Moreover, the hysteresis phenomenon is observed, i.e. the calculated impedance between charging steps is much more higher than impedance obtained between discharging steps at the same level of SoC. However, the biggest charge transfer resistance is noticed at 0% of SoC for both series of measurements. The hysteresis phenomenon is frequently observed in batteries, and its intensity depends on the cell type. When halting at the same state of charge during the charging and discharging of batteries, it implies that the ratio of specific vanadium ions remains constant, while many other parameters of the system vary more or less slightly. Discharging is a spontaneous process, whereas charging is a forced phenomenon. During the charging and discharging processes, distinct chemical reactions take place, and the potential of a specific electrode varies significantly between charging and discharging. Consequently, phenomena such as adsorption, temperature drift, capacitance, or induction effects are expected to differ between the charging and discharging phases of the cell, especially with porous electrodes. It is also important to note the phenomenon of relaxation, which is distinctly present in the studied batteries. Therefore, the hysteresis phenomenon in impedance measurements appears to be evident for batteries[49,50].

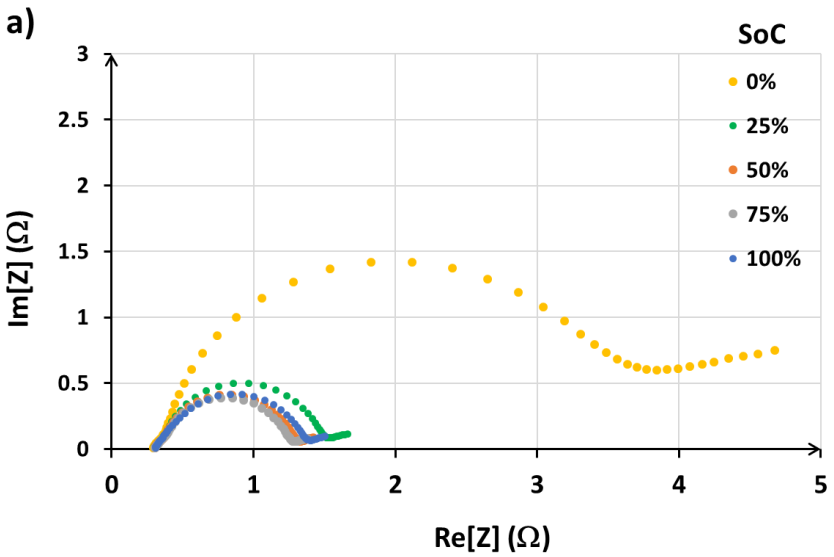

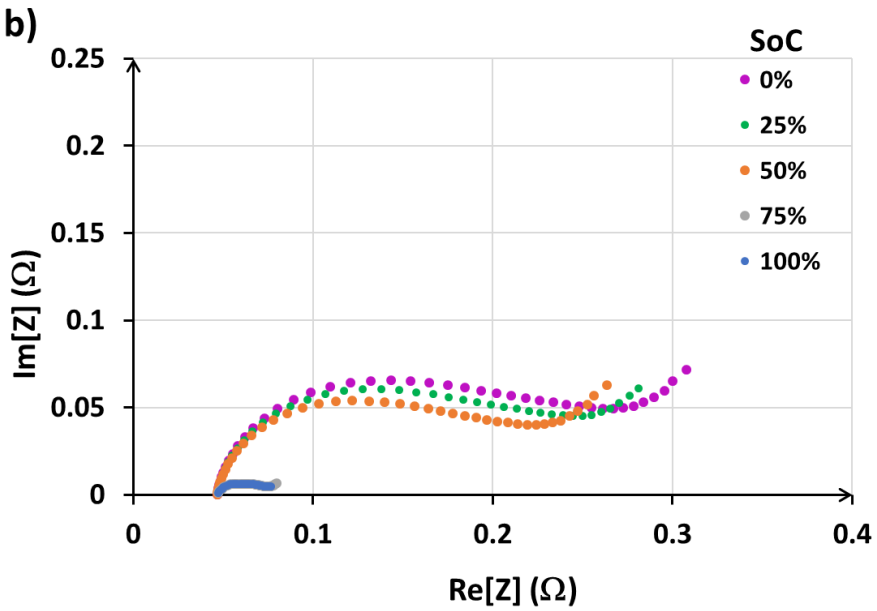

Figure 6. Nyquist plots obtained in the potentiostatic mode at various levels of state of charge: achieved during charging (a) or discharging (b) interruptions.

Note that during the galvanostatic EIS measurement, the DC current was not interrupted, and the obtained Nyquist plots are shown in Figure 7. The measurements were performed at the same levels of state of charge as in the potentiostatic mode: 0%, 25%, 50%, 75%, and 100% achieved during the charging or discharging process. The displayed spectra do not exhibit significant differences between the charging and discharging actions, as observed in the potentiostatic mode. Moreover, the impedance measurement conducted as the last of each series (i.e., at 100% SoC for charging and at 0% SoC for discharging processes) exhibits a noticeable deviation from the other measurements. These measurements are performed for very low concentration of reactants, so the measured impedances are visibly different and higher than for the previous spectra.

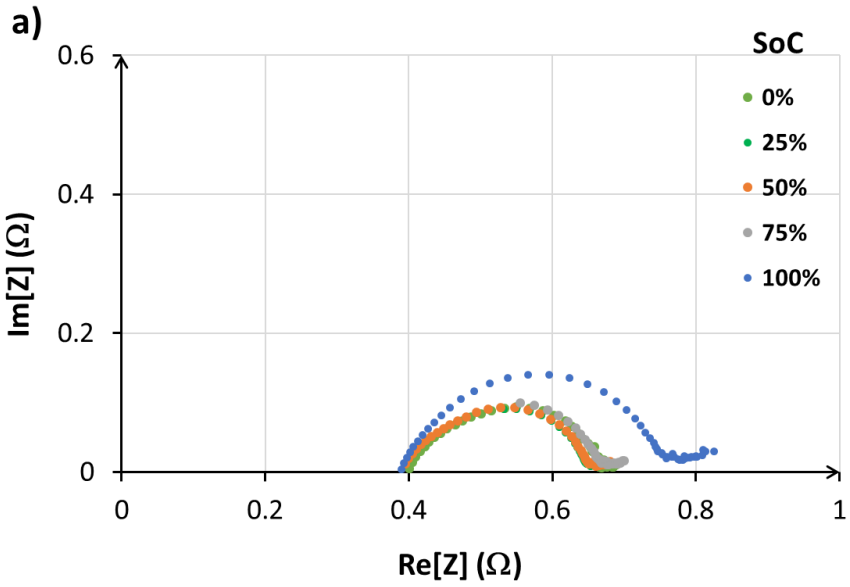

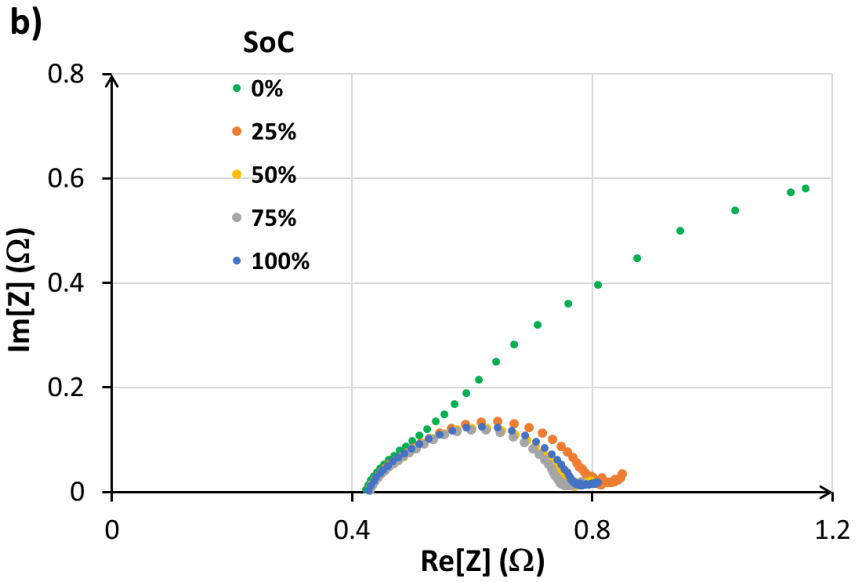

Figure 7. Nyquist plots obtained in the galvanostatic mode at various levels of state of charge (SoC): achieved during charging (a) or discharging (b).

The third mode of the used EIS measurements is foreseen for nonstationary systems operating in galvanostatic procedure. Decomposition of the multisinusoidal perturbation and response of the cell allow to record an averaged impedance spectrum for given measure duration. Figures 8a and 8b show obtained spectra of a system recording during charging and discharging process, respectively. The time variable is related to SoC level which can be also shown on the plot instead of time data. The Figure 8c presents the charging-discharging cycle for which DEIS measurements were performed. The columbic and voltage efficiencies of this cycle are 86.9% and 67.8%, respectively

a)

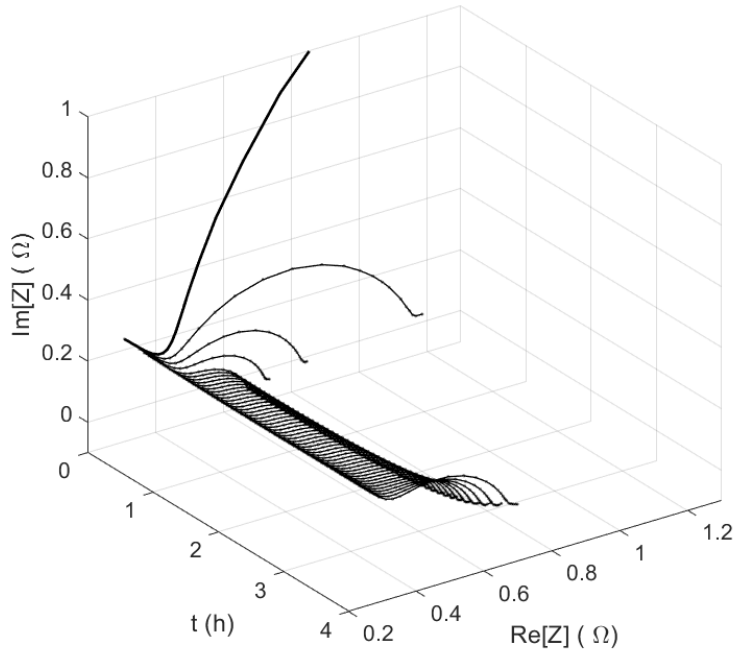
Im[Z] (Ω)
1
0.8
0.6
0.4
0.2
0
0
1
2
3
4
t (h)
0.2
0.4
0.6
0.8
1
1.2
Re[Z] (Ω)

b)

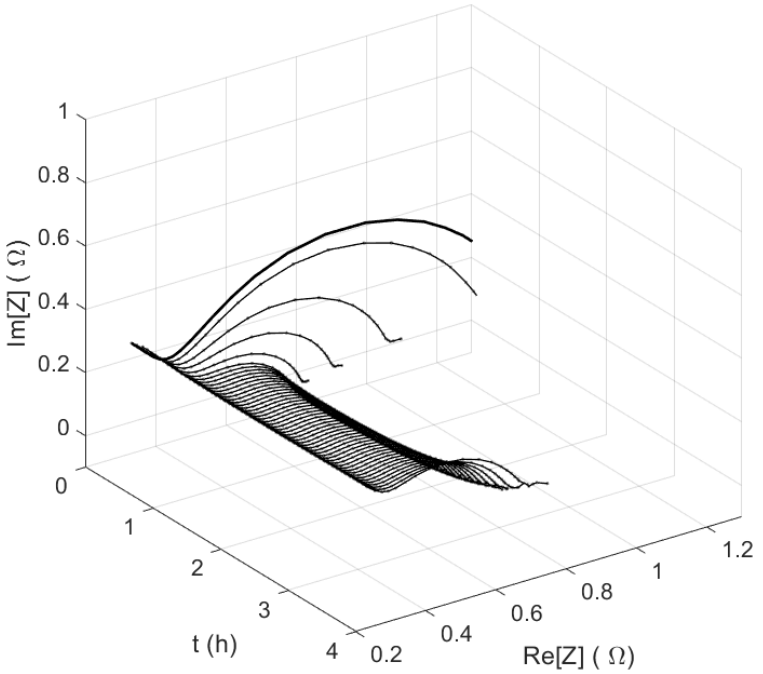
Im[Z] (Ω)
1
0.8
0.6
0.4
0.2
0
0
1
2
3
4
t (h)
0.2
0.4
0.6
0.8
1
1.2
Re[Z] (Ω)

c)

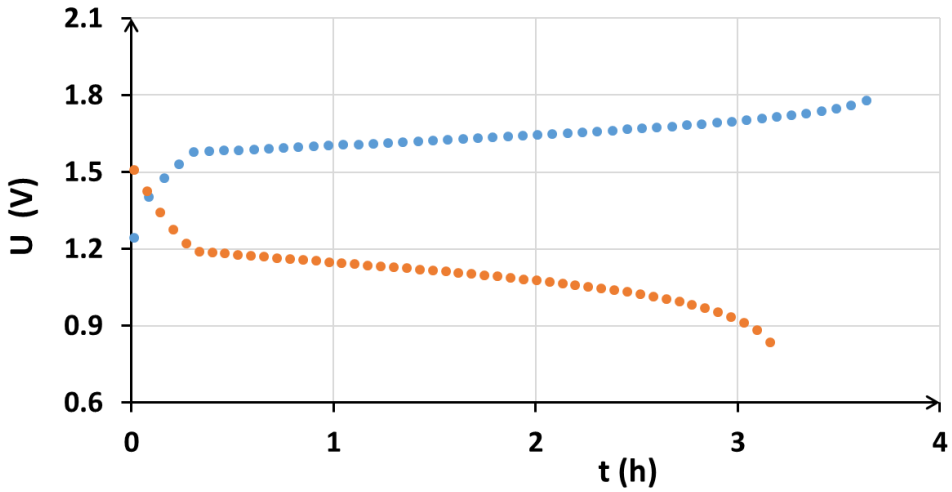

Figure 8. Nyquist plots obtained on a nonstationary all-vanadium redox flow battery system operating in galvanostatic mode: achieved during charging (a) and discharging (b); the charge-discharge (blue-orange points) performance recorded simultaneously with continuous DEIS measurements (c).

The impedance measurement presentations above consist of 50 individual spectra, each corresponding to a 2% change in state of charge. The number of displayed spectra can be adjusted according to specific requirements, but it is limited to the maximum allowable number, which is equivalent to the total number of recorded samples minus the number of samples included in a single spectrum.

The part of the spectrogram recorded for higher signal frequencies remains unchanged during battery operation. The opposite situation occurs for smaller frequency values. The highest impedance values are observed at the extreme states of charge, namely, 0% and 100% SoC, respectively. However, the highest impedance observed for a given procedure is noticed at its onset for both the charging and discharging phases. Most of the battery charging and discharging processes occur at comparable total impedance levels within the system, although slightly elevated values are evident during the discharging process. For easier comparison of the obtained data using the dynamic nonstationary mode of measurement with previous experimental data, Figures 9a and 9b present the Nyquist plots in the nonstationary mode for various levels of state of charge, i.e., 0%, 25%, 50%, 75%, and 100%.

At first glance, the spectra obtained during battery charging appear to be very similar to those obtained during battery discharging. The initial measured spectra exhibit visibly larger impedance values compared to the subsequent ones. Moreover, the discharging process shows slightly higher impedance compared to the charging process, as mentioned earlier in the description of the 3D graphs.

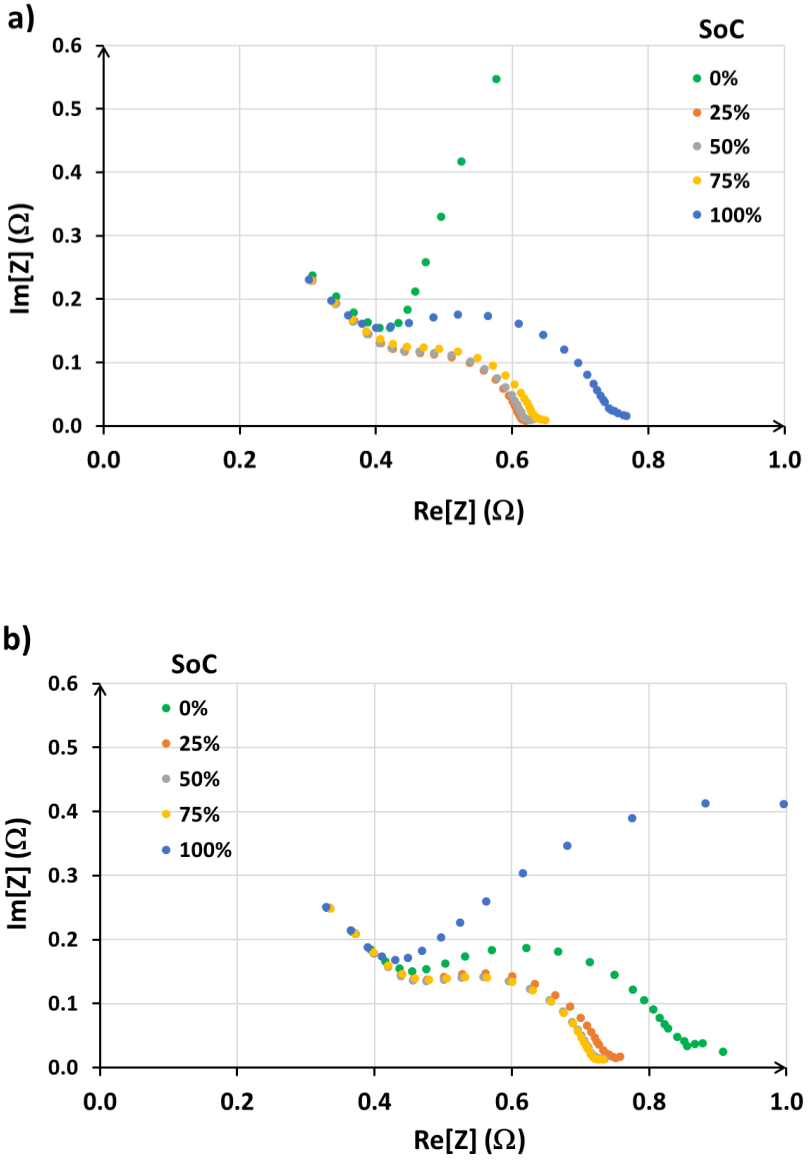

Figure 9. Nyquist plots obtained on a nonstationary all-vanadium redox flow battery system operating in galvanostatic mode: achieved during charging (a) and discharging (b) processes at level of 0, 25, 50, 75 and 100% of SoC.

The choice of measurement mode, whether galvanostatic or potentiostatic, depends on the specific characteristics of the system under investigation as well as the objectives and criteria of the experiment. In practice, it may be necessary to perform measurements in both modes to obtain a comprehensive understanding of the impedance characteristics of the electrochemical system. If the electrochemical properties of the system remain stable throughout the measurement, both potentiostatic and galvanostatic modes typically yield similar results. However, utilizing the galvanostatic mode can introduce additional complexity to the measurement process due to the often inadequate accuracy of the obtained results and the inability to control the potential effectively, resulting in uncontrolled polarization of the system under study. Galvanostatic measurements are less common because achieving accurate results in this mode requires the application of a complex and varied amplitude-controlled sequential excitation[51].

The goal of scientific research is to identify processes as accurately as possible, especially under conditions of their real operation. Therefore, each of the three measurement modes will show better or worse reflection of real operation. There is no doubt that measurement techniques enabling the study of processes during the operational life of a battery provide the most valuable insights into the properties of these systems. In this context, this study introduces an alternative continuous impedance measurement method, contrasting with the sequential potentiostatic measurements typically employed in the investigation of redox flow batteries. Additionally, cells rarely operate under potentiostatic conditions, especially near equilibrium conditions with low reaction rates (i.e., low polarizing current). Therefore, in the case of cells, galvanostatic measurements are more justified.

Impedance measurements in a two-electrode setup should be analyzed using equivalent circuits if the impedance of one electrode is negligibly small. In the case of a vanadium redox flow battery, both the cathodic and anodic processes are complex enough that attempting to fit a circuit to average out the processes seems unjustified and unnecessary, especially considering the intensive work being done on a three-electrode setup.

4. Conclusions

The authors present impedance measurement results in three modes. Classical impedance measurements under potentiostatic and galvanostatic conditions involved stopping battery operation, causing significant electrode potential changes compared to the working system (electrode potential changes are of over 200 mV). The kinetics of electrode reactions vary with potential, so impedance measurements reflect different system parameters. Dynamic measurements overcome this issue by enabling nonstationary electrode condition measurements without stopping cell operation, suitable for real-time monitoring. Spectral comparison shows less significant differences during charging and discharging, a departure from classical measurements. Therefore, the dynamic impedance measurement method emerges as the optimal approach for battery impedance studies. Future plans include interpreting results with equivalent circuits, especially for individual electrode spectra using reference electrodes. This requires developing a specialized redox flow cell, currently in progress.

[1] Bard A, Parsons R, Jordan J. Standard potentials in aqueous solution. New York: M. Dekker; 1985.

[2] Lasia A. Electrochemical impedance spectroscopy and its applications. Springer 2014;9781461489337:1–367. https://doi.org/10.1007/978-1-4614-8933-7.

[3] Lazanas AC, Prodromidis MI. Electrochemical Impedance Spectroscopy─A Tutorial. ACS Meas Sci Au 2023;3:162–93. https://doi.org/10.1021/ACSMEASURESCIAU.2C00070.

[4] Sadeghi E, Gholami MM, Hamzeh M, Alavi SMM, Saif M. A systematic overview of power electronics interfaced electrochemical impedance spectroscopy for energy storage systems. J Energy Storage 2023;62. https://doi.org/10.1016/J.EST.2023.106850.

[5] Pía Canales C. Electrochemical Impedance Spectroscopy and Its Applications. 21st Century Nanostructured Materials - Physics, Chemistry Classification, and Emerging Applications i Industry, Biomedicine, and Agriculture. IntechOpen; 2021. https://doi.org/10.5772/INTECHOPEN.101636.

[6] Wojcik PT, Orazem ME. Variable-Amplitude Galvanostatically Modulated Impedance Spectroscopy as a Tool for Assessing Reactivity at the Corrosion Potential Without Distorting Temporal Evolution of the System. Corrosion 1998;54:289–98. https://doi.org/10.5006/1.3284855.

[7] Harrington DA, Van Den Driessche P. Mechanism and equivalent circuits in electrochemical impedance spectroscopy. Electrochim Acta 2011;56:8005–13. https://doi.org/10.1016/J.ELECTACTA.2011.01.067.

[8] Blanke H, Bohlen O, Buller S, De Doncker RW, Fricke B, Hammouche A, et al. Impedance measurements on lead–acid batteries for state-of-charge, state-of-health and cranking capability prognosis in electric and hybrid electric vehicles. J Power Sources 2005;144:418–25. https://doi.org/10.1016/J.JPOWSOUR.2004.10.028.

[9] Watanabe H, Omoto S, Hoshi Y, Shitanda I, Itagaki M. Electrochemical impedance analysis on positive electrode in lithium-ion battery with galvanostatic control. J Power Sources 2021;507:230258. https://doi.org/10.1016/J.JPOWSOUR.2021.230258.

[10] Zappen H, Ringbeck F, Sauer DU. Application of Time-Resolved Multi-Sine Impedance Spectroscopy for Lithium-Ion Battery Characterization. Batteries 2018, Vol 4, Page 64 2018;4:64. https://doi.org/10.3390/BATTERIES4040064.

[11] Choi W, Shin HC, Kim JM, Choi JY, Yoon WS. Modeling and Applications of Electrochemical Impedance Spectroscopy (EIS) for Lithium-ion Batteries. J Electrochem Sci Technol 2020;11:1–13. https://doi.org/10.33961/JECST.2019.00528.

[12] Becker M, Turek T. Combination of impedance spectroscopy and potential probe sensing to characterize vanadium redox-flow batteries. J Power Sources 2020;446:227349. https://doi.org/10.1016/J.JPOWSOUR.2019.227349.

[13] Wan CTC, Ismail A, Quinn AH, Chiang YM, Brushett FR. Synthesis and Characterization of Dense Carbon Films as Model Surfaces to Estimate Electron Transfer Kinetics on Redox Flow Battery Electrodes. Langmuir 2023. https://doi.org/10.1021/acs.langmuir.2c03003.

[14] Aguiló-Aguayo N, Drozdzik T, Bechtold T. Impedance analysis of electrodes made of continuous carbon filaments in a 20 cm2 redox flow cell. J Electroanal Chem 2022;926:116954. https://doi.org/10.1016/J.JELECHEM.2022.116954.

[15] Jia C, Pan F, Zhu YG, Huang Q, Lu L, Wang Q. Energy Storage: High-energy density nonaqueous all redox flow lithium battery enabled with a polymeric membrane. Sci Adv 2015;1. https://doi.org/10.1126/sciadv.1500886.

[16] Milshtein JD, Barton JL, Carney TJ, Kowalski JA, Darling RM, Brushett FR. Towards Low Resistance Nonaqueous Redox Flow Batteries. J Electrochem Soc 2017;164:A2487–99. https://doi.org/10.1149/2.0741712JES.

[17] Smith KP, Rungta R, Wang AA, Monroe CW. Multi-Week Cycling of a Nonaqueous Flow Battery Using Tris-Bipyridine Iron (II) Triflate without Additional Supporting Electrolyte. J Electrochem Soc 2023;170:060510. https://doi.org/10.1149/1945-7111/ACD873.

[18] Loghavi MM, Zarei-Jelyani M, Babaiee M, Niknam Z, Eqra R. Graphene/Nafion ink-impregnated graphite felt for both positive and negative sides of enhanced vanadium redox flow battery. J Solid State Electrochem 2023;1:1–14. https://doi.org/10.1007/S10008-023-05476-Z.

[19] Köble K, Jaugstetter M, Schilling M, Braig M, Diemant T, Tschulik K, et al. Multimodal characterization of carbon electrodes' thermal activation for vanadium redox flow batteries. J Power Sources 2023;569:233010. https://doi.org/10.1016/J.JPOWSOUR.2023.233010.

[20] Mazur P, Mrlik J, Pocedic J, Vrana J, Dundalek J, Kosek J, et al. Effect of graphite felt properties on the long-term durability of negative electrode in vanadium redox flow battery. J Power Sources 2019;414:354–65. https://doi.org/10.1016/J.JPOWSOUR.2019.01.019.

[21] Jiang Y, Cheng G, Li Y, He Z, Zhu J, Meng W, et al. Promoting vanadium redox flow battery performance by ultra-uniform ZrO2@C from metal-organic framework. Chem Eng J 2021;415:129014. https://doi.org/10.1016/J.CEJ.2021.129014.

[22] Jiang QC, Li J, Yang YJ, Ren YJ, Dai L, Gao JY, et al. Ultrafine SnO2 in situ modified graphite felt derived from metal–organic framework as a superior electrode for vanadium redox flow battery. Rare Met 2023;42:1214–26. https://doi.org/10.1007/S12598-022-02228-2.

[23] Hu B, Seefeldt C, DeBruler C, Liu TL. Boosting the energy efficiency and power performance of neutral aqueous organic redox flow batteries. J Mater Chem A 2017;5:22137–45. https://doi.org/10.1039/C7TA06573F.

[24] Sun H, Yu M, Li Q, Zhuang K, Li J, Almheiri S, et al. Characteristics of charge/discharge and alternating current impedance in all-vanadium redox flow batteries. Energy 2019;168:693–701. https://doi.org/10.1016/J.ENERGY.2018.11.130.

[25] Choi C, Kim S, Kim R, Lee J, Heo J, Kim HT. In-situ observation of the degradation of all-vanadium redox flow batteries with dynamic hydrogen reference electrode under real operation conditions. J Ind Eng Chem 2019;70:355–62. https://doi.org/10.1016/J.JIEC.2018.10.036.

[26] Forner-Cuenca A, Penn EE, Oliveira AM, Brushett FR. Exploring the Role of Electrode Microstructure on the Performance of Non-Aqueous Redox Flow Batteries. J Electrochem Soc 2019;166:A2230–41. https://doi.org/10.1149/2.0611910JES.

[27] Manschke D, Seipp T, Berthold S, Friedrich KA. Verification of Redox Flow Batteries' Functionality by Electrochemical Impedance Spectroscopy Tests. Batter 2018;4:58. https://doi.org/10.3390/BATTERIES4040058.

[28] Sun C, Negro E, Nale A, Pagot G, Vezzù K, Zawodzinski TA, et al. An efficient barrier toward vanadium crossover in redox flow batteries: The bilayer [Nafion/(WO3)x] hybrid inorganic-organic membrane. Electrochim Acta 2021;378:138133. https://doi.org/10.1016/J.ELECTACTA.2021.138133.

[29] Trovò A, Zamboni W, Guarnieri M. Multichannel Electrochemical Impedance Spectroscopy and equivalent circuit synthesis of a large-scale vanadium redox flow battery. J Power Sources 2021;493:229703. https://doi.org/10.1016/J.JPOWSOUR.2021.229703.

[30] Creason SC, Smith DE. Fourier transform faradaic admittance measurements II. Ultra-rapid, high precision acquisition of the frequency response profile. J Electroanal Chem Interfacial Electrochem 1972;40:A1–5. https://doi.org/10.1016/S0022-0728(72)80146-3.

[31] Darowicki K. Theoretical description of the measuring method of instantaneous impedance spectra. J Electroanal Chem 2000;486:101–5. https://doi.org/10.1016/S0022-0728(00)00110-8.

[32] Ragoisha GA, Bondarenko AS. Potentiodynamic electrochemical impedance spectroscopy. Copper underpotential deposition on gold. Electrochem Commun 2003;5:392–5. https://doi.org/10.1016/S1388-2481(03)00075-4.

[33] Darowicki K, Ślepski P. Dynamic electrochemical impedance spectroscopy of the first order electrode reaction. J Electroanal Chem 2003;547:1–8. https://doi.org/10.1016/S0022-0728(03)00154-2.

[34] Darowicki K, Orlikowski J, Arutunow A. Detection of stress corrosion cracking dynamics by dynamic electrochemical impedance spectroscopy. Corros Eng, Sci Technol 2004;39(3):255-60. https://doi.org/10.1179/147842204X2844.

[35] Darowicki K, Krakowiak S, Slepski P. The time dependence of pit creation impedance spectra. Electrochem Commun 2004;6:860–6. https://doi.org/10.1016/j.elecom.2004.06.010.

[36] Darowicki K, Kawula J. Dynamic electrochemical impedance spectroscopy of the adsorption and relaxation of polyaniline chains during potentiodynamic redox transformations. Russ J Electrochem 2007;43:1055–63. https://doi.org/10.1134/S1023193507090091.

[37] Darowicki K, Zieliński A, Kurzydłowski KJ. Application of dynamic impedance spectroscopy to atomic force microscopy. Sci Technol Adv Mater 2008;9(4). https://doi.org/10.1088/1468-6996/9/4/045006.

[38] Darowicki K, Andrearczyk K. Determination of occurrence of anodic excursion peaks by dynamic electrochemical impedance spectroscopy, atomic force microscopy and cyclic voltammetry. J Power Sources 2009;189(2):988–93. https://doi.org/10.1016/J.JPOWSOUR.2009.01.039.

[39] Darowicki K, Andrearczyk K, Slepski P, Sierczynska A, Lota G, Fic K, et al. Determination of Pseudocapacitance Changes of Nickel Oxide NiO Electrode with the Use of Dynamic Electrochemical Impedance Spectroscopy. Int J Electrochem Sci 2014;9(4):1702–14. https://doi.org/10.1016/S1452-3981(23)07884-7.

[40] Ryl J, Bogdanowicz R, Slepski P, Sobaszek M, Darowicki K. Dynamic Electrochemical Impedance Spectroscopy (DEIS) as a Tool for Analyzing Surface Oxidation Processes on Boron-Doped Diamond Electrodes. J Electrochem Soc 2014;161:H359–64. https://doi.org/10.1149/2.016406JES.

[41] Niedzialkowski P, Slepski P, Wysocka J, Chamier-Cieminska J, Burczyk L, Sobaszek M, et al. Multisine impedimetric probing of biocatalytic reactions for label-free detection of DEFB1 gene: How to verify that your dog is not human? Sensors Actuators B Chem 2020;323:128664. https://doi.org/10.1016/J.SNB.2020.128664.

[42] Darowicki K, Ślepski P, Szociński M. Novel application of dynamic electrochemical impedance monitoring to a cataphoretic coating process. Prog Org Coatings 2020;149:105906. https://doi.org/10.1016/J.PORGCOAT.2020.105906.

[43] Lipinska W, Ryl J, Slepski P, Siuzdak K, Grochowska K. Exploring multi-step glucose oxidation kinetics at GOx-functionalized nanotextured gold surfaces with differential impedimetric technique. Measurement 2021;174:109015. https://doi.org/10.1016/j.measurement.2021.109015.

[44] Brodowski M, Pierpaoli M, Janik M, Kowalski M, Ficek M, Slepski P, et al. Enhanced susceptibility of SARS-CoV-2 spike RBD protein assay targeted by cellular receptors ACE2 and CD147: Multivariate data analysis of multisine impedimetric response. Sensors Actuators B Chem 2022;370:132427. https://doi.org/10.1016/J.SNB.2022.132427.

[45] Slepski P, Janicka E, Darowicki K, Pierozynski B. Impedance monitoring of fuel cell stacks. J Solid State Electrochem 2015;19:929–33. https://doi.org/10.1007/S10008-014-2676-8/FIGURES/7.

[46] Darowicki K, Janicka E, Mielniczek M, Zielinski A, Gawel L, Mitzel J, et al. The influence of dynamic load changes on temporary impedance in hydrogen fuel cells, selection and validation of the electrical equivalent circuit. Appl Energy 2019;251:113396. https://doi.org/10.1016/J.APENERGY.2019.113396.

[47] Slepski P, Darowicki K, Andrearczyk K. On-line measurement of cell impedance during charging and discharging process. J Electroanal Chem 2009;633(1):121–6. https://doi.org/10.1016/J.JELECHEM.2009.05.002.

[48] Huang J, Li Z, Zhang J. Dynamic electrochemical impedance spectroscopy reconstructed from continuous impedance measurement of single frequency during charging/discharging. J Power Sources 2015;273(1):1098–102. https://doi.org/10.1016/J.JPOWSOUR.2014.07.067.

[49] Oldenburger M, Bedürftig B, Gruhle A, Grimsmann F, Richter E, Findeisen R, et al. Investigation of the low frequency Warburg impedance of Li-ion cells by frequency domain measurements. J Energy Storage 2019;21:272–80. https://doi.org/10.1016/J.EST.2018.11.029.

[50] Van Der Ven A, See KA, Pilon L. Hysteresis in electrochemical systems. Batter Energy 2022;1:20210017. https://doi.org/10.1002/BTE2.20210017.

[51] Wojcik PT, Agarwal P, Orazem ME. A method for maintaining a constant potential variation during galvanostatic regulation of electrochemical impedance measurements. Electrochim Acta 1996;41(7-8):977–83. https://doi.org/10.1016/0013-4686(95)00428-9.